

FORMAL VERIFICATION OF OCTOROTOR FLIGHT ENVELOPE USING BARRIER FUNCTIONS AND SMT SOLVING

BYRON HEERSINK, PAPE SYLLA, AND MICHAEL A. WARREN

ABSTRACT. This paper introduces an approach for formally verifying the safety of the flight controller of an octorotor platform. Our method involves finding regions of the octorotor's state space that are considered safe, and which can be proven to be invariant with respect to the dynamics. Specifically, exponential barrier functions are used to construct candidate invariant regions near desired commanded states. The proof that these regions are invariant is discovered automatically using the dReal SMT solver, which ensures the accurate command tracking of the octorotor to within a certain margin of error. Rotor failures in which rotor thrusts become stuck at fixed values are considered and accounted for via a pseudo-inverse control allocator. The safety of the control allocator is verified in dReal by checking that the thrusts demanded by the allocator never exceed the capability of the rotors. We apply our approach on a specific octorotor example and verify the desired command tracking properties of the controller under normal conditions and various combinations of rotor failures.

1. INTRODUCTION

Recently, interest in the study of multirotor air vehicles has been growing quickly due to their high maneuverability and many applications, such as inspection and surveillance. In particular, the quadrotor has been a popular platform with which to conduct UAV (unmanned aerial vehicle) research. While the quadrotor can tolerate partial rotor faults (see, e.g., [23, 32, 20, 31]), it becomes uncontrollable if one of its rotors fails completely (though [5] shows that only yaw control need be lost). Thus the octorotor has been studied as an alternative that is more robust to rotor failures [14, 1, 2, 21, 22].

An approach to addressing flight safety for UAVs in a number of recent works has been through the use of control barrier functions (CBFs). A CBF is a scalar-valued function on the state space of a control system whose support (here understood as the region where the function attains positive values) is forward invariant under appropriate controls. Thus, one can (mathematically) guarantee the safety of the system by finding a CBF with support contained in a safe region of the state space. In particular, in [24], CBFs are used to ensure that teams of quadrotors are able to fly in a collision free manner; in [18], CBFs are used for obstacle avoidance in quadrotor path planning in a surveillance scenario; and in [28], CBFs are used for flight safety for quadrotors under some degree of human control. Other works using barrier functions for UAV safety include [27, 26, 11]. Other applications of barrier functions include adaptive cruise control and lane keeping [4, 30, 29], bipedal walking robots [16, 15], and collision avoidance for multirobot systems on land [25]. See [3] for a survey of control barrier functions.

Instead of utilizing barrier functions within control algorithms to ensure safety, as in the aforementioned references, the focus of this paper is to use barrier functions to analyze the safety properties of conventionally defined controllers. Specifically, our aim is to provide a method of verifying the safety of controllers using satisfiability modulo theories (SMT) solving. Our work is in the spirit of [9, 10], in which controllers for flight vehicles are designed, and the flight envelope and asymptotic stability of the controller are verified by the automated theorem prover MetiTarski. However, in these works, the design of the controllers is fairly specialized, and is closely tied together with how the controller’s safety is verified. As above, a principal goal of our work is to decouple safety analysis from controller design so that our techniques can be employed even in cases where the underlying controller can no longer be modified or where it is for other reasons not feasible to incorporate barrier functions at the design stage.

The goal of this paper is therefore to introduce another approach to the formal verification of the flight envelope of a UAV, one particularly that has the potential to be used in a way that is independent of the design of the controller. Our core method involves the use of barrier functions, more specifically exponential barrier functions [17] of a certain form, to produce an invariant subset of a prescribed safe region near a desired commanded point in the control system’s state space (e.g., as one might see in connection with gain scheduling). Our method aims to analyze systems with a controller designed to track commands and whose dynamics can be approximated reasonably well by the linearization around a desired operating state. In particular, our approach lends itself well to analyzing UAV safety in states where the vehicle is nearly upright or mildly tilting. It also has potential for use in the verification of gain scheduled controllers that are currently in common use for many kinds of aircraft.

The specific type of UAV we analyze is an octorotor, which, as mentioned above, is robust to rotor failures. This allows us to address the issue of fault tolerance in our approach. We account for complete rotor failures, in which one or more rotors stop working entirely and exert zero thrust, and more generally failures in which rotors become stuck at specific speeds. To mitigate these failures, we utilize a simple control allocator to attempt to maintain the ideal octorotor behavior. The main property of the control allocator that needs to be verified is that the rotors are always capable of exerting the rotor thrusts commanded by the allocator. We assume that failures are perfectly known, and do not address the issue of fault detection, as in [21, 22].

In Section 2, we present the equations of motion of the octorotor model we study. In Section 3, we describe the controller. This includes an explanation of the kinds of rotor failures considered and how they are accounted for by the control allocator. Section 4 introduces the general barrier function framework employed, and Section 5 describes precisely the form of barrier functions used for the octorotor. In Section 6, we formulate in detail the properties that are analyzed in dReal and that confirm the desired safety properties of the octorotor controller. In Section 7, we describe the results obtained for a specific controller: we formally verify that the octorotor will follow commands closely in spite of dynamic disturbances when functioning normally and under various rotor failures, and we identify some combinations of rotor failures in which the desired conditions are violated. Finally, concluding remarks are found in Section 8.

2. OCTOROTOR DYNAMICS MODEL

In this section, we describe the octorotor dynamics model that we analyze. We follow [7, 12] in modeling the rigid body dynamics and some characteristics of the rotors, and our octorotor model is based on that in [14]. See also [13] for an introduction to the modeling of multicopter aerial vehicles. The octorotor consists of eight identical rotors arranged in the shape of a regular octagon as illustrated in Figure 1. Each rotor exerts an upward thrust normal to the plane of the octorotor, and a torque about the octorotor's center of mass as explained below.

To express the octorotor's dynamics, we first describe the two reference frames required. First, the world reference frame, which we assume is inertial, is given by the standard unit basis vectors $e_1 = [1, 0, 0]^T$, $e_2 = [0, 1, 0]^T$, and $e_3 = [0, 0, 1]^T$. We assume that e_1 points north, e_2 points east, and e_3 points down. Next, we assume that the body of the octorotor has reference frame given by the orthonormal (vertical) vectors b_1, b_2, b_3 , where b_1 is considered the forward direction with respect to the octorotor, b_2 is the right direction, and b_3 is the down direction. (In Figure 1, b_3 points into the page.) The 3×3 matrix $[b_1, b_2, b_3]$ is denoted by R , which is the rotation matrix from the body frame to the world frame.

Now we describe the state space of the system. We denote the inertial position of the octorotor's center of mass by $r = [x, y, z]^T$; and the inertial velocity by $v = [v_x, v_y, v_z]^T$. Another component of the state of the octorotor is its orientation, which is given by R . Alternatively, we express the orientation in terms of Euler angles. Letting ϕ, θ, ψ be the roll, pitch, and yaw angles, respectively, corresponding to the Z - Y - X sequence for Euler angles, we have the following relationship between R and $[\phi, \theta, \psi]$:

$$\begin{aligned} R &= \begin{bmatrix} c_\psi & -s_\psi & 0 \\ s_\psi & c_\psi & 0 \\ 0 & 0 & 1 \end{bmatrix} \begin{bmatrix} c_\theta & 0 & s_\theta \\ 0 & 1 & 0 \\ -s_\theta & 0 & c_\theta \end{bmatrix} \begin{bmatrix} 1 & 0 & 0 \\ 0 & c_\phi & -s_\phi \\ 0 & s_\phi & c_\phi \end{bmatrix} \\ &= \begin{bmatrix} c_\theta c_\psi & s_\phi s_\theta c_\psi - c_\phi s_\psi & c_\phi s_\theta c_\psi + s_\phi s_\psi \\ c_\theta s_\psi & s_\phi s_\theta s_\psi + c_\phi s_\psi & c_\phi s_\theta s_\psi - s_\phi c_\psi \\ -s_\theta & s_\phi c_\theta & c_\phi c_\theta \end{bmatrix}. \end{aligned}$$

Here and below, we let $s_* = \sin(*)$, $c_* = \cos(*)$, and $t_* = \tan(*)$. The final component of the state space is the angular velocity vector $\Omega = [\Omega_1, \Omega_2, \Omega_3]^T$ of the octorotor with respect to the body reference frame.

Next, we describe the control space of the octorotor. The control space consists of the eight rotors, each of which exerts a force and torque on the octorotor. For simplicity, we assume that the thrust of each rotor can be directly set, and we do not model the motor dynamics. Also, we assume that each rotor can rotate only in one direction as shown in Figure 1, and that the thrust exerted is in the upward direction $-b_3$ with respect to the octorotor. Let f_j , $j = 1, \dots, 8$, denote the forces exerted by the rotors. We assume that each f_j is restricted to an interval $[f_{min}, f_{max}]$, where f_{min} and f_{max} are the least and greatest possible forces that each rotor can exert on the octorotor, respectively. Since we are assuming that the rotors can only rotate in one direction, we have $f_{min} \geq 0$. Let d denote the distance from the center of mass of the octorotor to the center of each rotor, and note that the thrust of the j th rotor induces a torque of magnitude $d \cdot f_j$ about an axis in the octorotor plane perpendicular to the arm containing the rotor. The j th rotor also induces a torque about the b_3 axis of magnitude $c \cdot f_j$, where c is the ratio

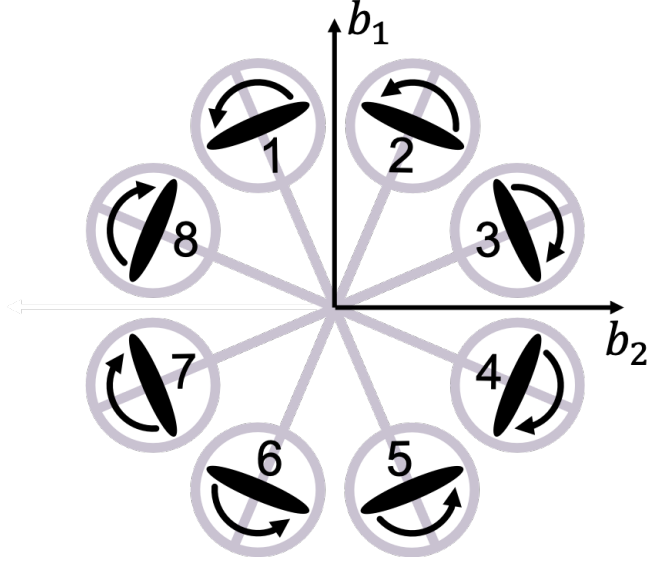


FIGURE 1. Octorotor diagram

of induced torque to thrust. In particular, the rotors that rotate counterclockwise induce a torque in the direction of b_3 , and those that rotate clockwise induce a torque in the direction of $-b_3$.

Let F denote the total thrust exerted by the rotors, and let τ_1, τ_2, τ_3 denote the net torque exerted by the rotors about the body axes b_1, b_2, b_3 , respectively. Then letting $\gamma = \frac{\pi}{8}$, the relationship between $u = [F, \tau_1, \tau_2, \tau_3]^T$ and $f_{all} = [f_1, f_2, \dots, f_8]^T$ is given by $u = \Lambda f_{all}$, where Λ is the matrix

$$\begin{bmatrix} 1 & 1 & 1 & 1 & 1 & 1 & 1 & 1 \\ ds_\gamma & -ds_\gamma & -dc_\gamma & -dc_\gamma & -ds_\gamma & ds_\gamma & dc_\gamma & dc_\gamma \\ dc_\gamma & dc_\gamma & ds_\gamma & -ds_\gamma & -dc_\gamma & -dc_\gamma & -ds_\gamma & ds_\gamma \\ c & c & -c & -c & c & c & -c & -c \end{bmatrix}.$$

Next, let $m \in \mathbb{R}$ denote the mass of the octorotor, $g = 9.81 \frac{\text{m}}{\text{s}^2}$ be the gravitational acceleration, and

$$J = \begin{bmatrix} J_1 & 0 & 0 \\ 0 & J_2 & 0 \\ 0 & 0 & J_3 \end{bmatrix}$$

be the inertia matrix of the octorotor with respect to its body frame. Then let $\Delta_r = [\Delta_x, \Delta_y, \Delta_z]^T$ and $\Delta_R = [\Delta_{R,1}, \Delta_{R,2}, \Delta_{R,3}]^T$ denote unstructured force and torque disturbances due to dynamics that are unaccounted for. In particular, we view these disturbances as encompassing aerodynamic effects such as air drag and blade flapping, which, for simplicity, we do not model in detail. (See, e.g., [8, 13] for more information.) We assume the disturbances are unknown, untracked, and measurable functions of time, and satisfy the inequalities $|\Delta_x|, |\Delta_y|, |\Delta_z| \leq \Delta_{r,max}$, and $|\Delta_{R,1}|, |\Delta_{R,2}| \leq \Delta_{R,12,max}$, $|\Delta_{R,3}| \leq \Delta_{R,3,max}$, where $\Delta_{r,max}$, $\Delta_{R,12,max}$, and $\Delta_{R,3,max}$ are fixed bounds. Then the differential equations describing the motion

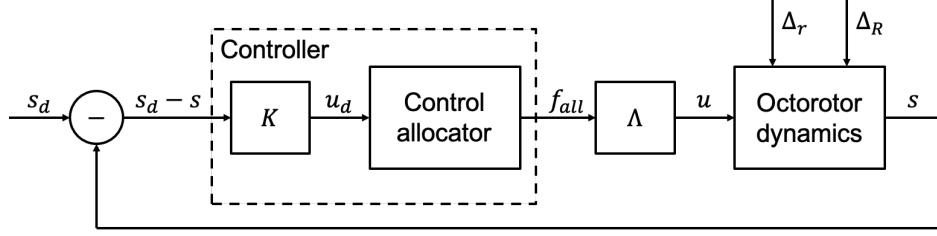


FIGURE 2. Octorotor system block diagram

of the octorotor are

$$\begin{aligned} \dot{r} &= v \\ m\dot{v} &= \begin{bmatrix} 0 \\ 0 \\ mg \end{bmatrix} - F \begin{bmatrix} c_\phi s_\theta c_\psi + s_\phi s_\psi \\ c_\phi s_\theta s_\psi - s_\phi c_\psi \\ c_\phi c_\theta \end{bmatrix} + \Delta_r \\ \begin{bmatrix} \dot{\phi} \\ \dot{\theta} \\ \dot{\psi} \end{bmatrix} &= \begin{bmatrix} 1 & s_\phi t_\theta & c_\phi t_\theta \\ 0 & c_\phi & -s_\phi \\ 0 & \frac{s_\phi}{c_\theta} & \frac{c_\phi}{c_\theta} \end{bmatrix} \begin{bmatrix} \Omega_1 \\ \Omega_2 \\ \Omega_3 \end{bmatrix} \\ J\dot{\Omega} &= \tau - \Omega \times J\Omega + \Delta_R. \end{aligned}$$

In this paper, we focus on the dynamics of the components of the state vector

$$s = [v_z, \phi, \theta, \psi, \Omega_1, \Omega_2, \Omega_3]^T,$$

which we consider to be the “inner loop” components of the octorotor system. Note that the derivative of these components do not depend on $[x, y, z, v_x, v_y]$, and so we may safely view the components of s as forming the state space of a well-defined control system.

3. CONTROLLER

As mentioned above, we focus on controlling the dynamics of the octorotor’s vertical velocity and orientation. In particular, the controller we use is designed to have the components $(v_z, \phi, \theta, \psi)$ of the octorotor state track the command $(v_{z,d}, \phi_d, \theta_d, \psi_d)$. In other words, we wish for s to track $s_d = [v_{z,d}, \phi_d, \theta_d, \psi_d, 0, 0, 0]^T$. The block diagram of the full control system is shown in Figure 2.

The controller consists of two components. The first, block K in the diagram, takes as input the difference $s_d - s$ between the current state and the commanded state, and returns the commanded vector $u_d = [F_d, \tau_{1,d}, \tau_{2,d}, \tau_{3,d}]^T$ of net force and torques. This component disregards whether the octorotor is actually capable of executing u_d , that is, whether there exists a valid f_{all} which yields the desired command. So u_d is not necessarily the actual control input $u = [F, \tau_1, \tau_2, \tau_3]^T$. To find u , we include a second component, the control allocator, which takes u_d as input and returns a value for f_{all} such that $f_{min} \leq f_j \leq f_{max}$ for all j and the resulting control input $u = \Lambda f_{all}$ is intended to equal, or be close to, u_d . Note additionally that we use the control allocator to implement rotor failures. Specifically, we assume that the rotor failures are always known and the control allocator is defined so that the thrusts f_j corresponding to the failed rotors match the values at which they are stuck.

While under some circumstances the commanded value u_d is not equal to u , we want to ensure this never happens for the purposes of verifying safety. In particular, we wish to find an invariant set for which all the commanded values u_d can be executed by the octorotor. This allows us to split up our verification procedure into 2 separate steps as follows. The first step is to verify that a chosen candidate invariant set is rendered invariant by the controller under the assumption that u is always equal to u_d . The second step is to verify that the equality $u = u_d$ is in fact satisfied for the control allocator for all states in the candidate invariant set. This step is done for each rotor failure combination analyzed.

3.1. Controller block K . The block K controller component has a simple PD structure very similar to [14], and is defined by the following:

$$(1) \quad \begin{aligned} F_d &= \frac{mg}{c_\phi c_\theta} + K_{dz}(v_z - v_{z,d}) \\ \tau_{1,d} &= -K_{p\phi}(\phi - \phi_d) - K_{d\phi}\Omega_1 \\ \tau_{2,d} &= -K_{p\theta}(\theta - \theta_d) - K_{d\theta}\Omega_2 \\ \tau_{3,d} &= -K_{p\psi}(\psi - \psi_d) - K_{d\psi}\Omega_3. \end{aligned}$$

Note that $mg/c_\phi c_\theta$ is the total rotor thrust needed to keep the vertical acceleration of the octorotor at 0. We take the various coefficients K . from a linear quadratic regulator that we compute for the linearized octorotor dynamics at $s = 0$, and under the assumption that $v_{z,d}, \phi_d, \theta_d, \psi_d, \Delta_{r,max}, \Delta_{R,12,max}, \Delta_{R,3,max}$ are all equal to 0.

3.2. Control allocator. To find the individual rotor thrusts exerted by the octorotor in response to the commanded control input u_d , we use a simple pseudo-inverse control allocation method (see [19]). At this stage, we account for the possibility that some of the rotors have failed. So let $W \subseteq \{1, \dots, 8\}$ be the (possibly empty) set of indices corresponding to rotors that have failed, and for $j \in W$, let $\bar{f}_j \in [f_{min}, f_{max}]$ be thrust at which rotor j is stuck. Also let $\bar{f}_j = 0$ for $j \notin W$ and $\bar{f}_{all} = [\bar{f}_1, \dots, \bar{f}_8]^T$. Next, define Λ_W to be the matrix with the same entries as Λ , except that column j of Λ_W is zeroed out for all $j \in W$. Then let Λ_W^\dagger be the pseudo-inverse of Λ_W . Now we define $\tilde{f}_{all} = [\tilde{f}_1, \dots, \tilde{f}_8]^T$ by

$$(2) \quad \tilde{f}_{all} = \bar{f}_{all} + \Lambda_W^\dagger(u_d - \Lambda \bar{f}_{all}).$$

The vector \tilde{f}_{all} consists of potential rotor values, with $\tilde{f}_j = \bar{f}_j$ for all $j \in W$ as required. However, it is possible that \tilde{f}_j falls outside $[f_{min}, f_{max}]$ for some $j \notin W$. We thus define f_j for $j = 1, \dots, 8$ by

$$f_j = \begin{cases} \bar{f}_j & \text{if } j \in W \\ \text{mid}\{f_{min}, \tilde{f}_j, f_{max}\} & \text{if } j \notin W, \end{cases}$$

where $\text{mid}\{f_{min}, \tilde{f}_j, f_{max}\}$ denotes the middle value of the set $\{f_{min}, \tilde{f}_j, f_{max}\}$. Thus $f_j \in [f_{min}, f_{max}]$ for all $j \notin W$, and so we let $f_{all} = [f_1, \dots, f_8]^T$. This completes the definition of the control allocator.

To conclude this section, we wish to describe conditions for which $u = u_d$. We first note that the matrix Λ_W is of rank 4 if $|W| < 4$, or $|W| = 4$ and W is not equal to $\{1, 2, 3, 8\}$, $\{1, 2, 4, 7\}$, $\{1, 2, 5, 6\}$, or any index set that can be obtained from one of these sets by increasing each element by a common even number and taking the remainder upon division by 8 when necessary. (This is equivalent to

rotating the rotor failure patterns corresponding to the 3 sets about the octorotor center by multiples of 90 degrees.) When Λ_W is of rank 4, we have $\Lambda_W \Lambda_W^\dagger = I_{4 \times 4}$ and $\Lambda \tilde{f}_{all} = u_d$. So to determine whether $u = u_d$, it suffices to check whether $\tilde{f}_j \in [f_{min}, f_{max}]$ for all $j \notin W$, and this is the condition we use, since we only consider scenarios with up to 2 rotor failures.

4. BARRIER FUNCTIONS

The safety conditions that we wish to prove rely on the notion of invariant sets. An invariant set for a dynamical system is a region I of the state space of the system such that if the state begins in I , then the state remains in I at all future times. Our goal is to ensure that for all commands s_d one wishes to give the octorotor, there exists an invariant set of octorotor states s which are close to s_d . Obtaining and verifying such invariant sets allows one to gauge with certainty how close the controller is able to keep the octorotor state to the given commands in spite of the disturbances given in the dynamics model.

To find these invariant sets, we utilize barrier functions. The type of barrier function we use is a form of exponential barrier function as introduced by [17]. (See, in particular, Remark 5, Proposition 1, and the related discussion.) With this concept, we find a set of linear inequalities on the state space which forms a candidate invariant region which we can verify. In this section, we provide a brief overview of the reasoning behind exponential barrier functions, and then explain the general form of exponential barrier functions we use.

Let $\dot{x} = f(x)$ define a dynamical system on some set $X \subseteq \mathbb{R}^n$, and let $h = h_0 : X \rightarrow \mathbb{R}$ be a differentiable function. The basic logic underlying exponential barrier functions is that, for a trajectory $x(t)$ of the dynamical system, $h(x(t)) \geq 0$ for all $t \geq 0$ whenever $h(x(0)) \geq 0$ and

$$\begin{aligned} & \frac{d}{dt}(h(x(t))) + p_1 h(x(t)) \\ & = (\nabla h)(x(t)) \cdot f(x(t)) + p_1 h(x(t)) \geq 0 \end{aligned}$$

for all $t \geq 0$, where $p_1 > 0$ is a constant. Thus, if one seeks an invariant subset of $\{x \in X : h(x) \geq 0\}$, one can, if necessary, enforce the extra inequality $h_1(x) := (\nabla h)(x) \cdot f(x) + p_1 h(x) \geq 0$, and form the set $\{x \in X : h_0(x), h_1(x) \geq 0\}$. If one can then prove that whenever the initial condition is chosen from this set, the inequality $h_1(x) \geq 0$ holds indefinitely, then $h_0(x) \geq 0$ holds automatically. One can furthermore inductively form a sequence of functions h_j defined by $h_j(x) = (\nabla h_{j-1})(x) \cdot f(x) + p_j h_{j-1}(x)$ and examine the sets $\{x \in X : h_j(x) \geq 0, j = 0, \dots, n\}$ to see if any of them are invariant, and in particular, checking if the inequality $h_n(x) \geq 0$ holds indefinitely when $h_0(x), \dots, h_n(x) \geq 0$ holds at the initial condition. See [17] for more details regarding the reasoning above in the context of controlled dynamical systems.

In light of the above discussion, we now explain the general barrier function framework we use in constructing invariant sets for the octorotor. It relies on a few starting assumptions. First, we assume that a controller is already in place (namely, one of the form described in Section 3), which seeks to track a fixed commanded state, and the dynamics are governed by a differential equation of the form $\dot{x} = f(x, x_d, d)$, where $x \in \mathbb{R}^n$ is the state, $x_d \in \mathbb{R}^d$ is the commanded state, $d \in \mathbb{R}^m$ denotes any potential disturbances (all three being vertical vectors), and

f is Lipschitz on any candidate invariant set of interest. Next, we assume that the dynamics can be approximated sufficiently well by a linearization of the form $\dot{x} = A(x - x_d)$, $A \in \mathbb{R}^{n \times n}$. In the case of the octorotor, we assume A results from the linearization of the dynamics where $s = 0$. Next, we assume that the conditions we desire to be enforced are of the form $P_i(x - x_d) + D_i \geq 0$, where P_i is a horizontal vector of length n , and D_i is a positive scalar. The aim of these inequalities is to form a starting set of states x nearby x_d in which to find an invariant set. The goal is then to confirm the ability of the controller to keep the state x near x_d .

Now we form a sequence of barrier functions that aim to enforce $P_i(x - x_d) + D_i \geq 0$. First, we let $p_{i,j}, \delta_{i,j} \geq 0$ be constants for $j = 1, \dots, n_i$ such that $\sum_{j=1}^{n_i} \delta_{i,j} < D_i$. Then we define the sequence of functions

$$\begin{aligned} \tilde{h}_{i,0}(x) &= P_i(x - x_d) + D_i \\ \tilde{h}_{i,1}(x) &= P_i(I + p_{i,1}A)(x - x_d) + D_i - \delta_{i,1} \\ \tilde{h}_{i,2}(x) &= P_i(I + p_{i,1}A)(I + p_{i,2}A)(x - x_d) \\ &\quad + D_i - \delta_{i,1} - \delta_{i,2} \\ &\quad \vdots \\ \tilde{h}_{i,n_i}(x) &= P_i(I + p_{i,1}A) \cdots (I + p_{i,n_i}A)(x - x_d) \\ &\quad + D_i - \delta_{i,1} - \cdots - \delta_{i,n_i}. \end{aligned}$$

where I is the $n \times n$ identity matrix. Notice that under the linear dynamics, $\tilde{h}_{i,j}(x) \leq \tilde{h}_{i,j-1}(x) + p_{i,j} \frac{d}{dt}(\tilde{h}_{i,j-1}(x))$ for $j = 1, \dots, n_i$, and so if the inequality $\tilde{h}_{i,j} \geq 0$ holds, then $\tilde{h}_{i,j-1}$ holds automatically. Next, we let $\mu > 0$ be a parameter and form our barrier function sequence

$$\begin{aligned} h_{i,0,\mu}(x) &= \frac{P_i(x - x_d)}{D_i} + \mu \\ h_{i,1,\mu}(x) &= \frac{P_i(I + p_{i,1}A)(x - x_d)}{D_i - \delta_{i,1}} + \mu \\ h_{i,2,\mu}(x) &= \frac{P_i(I + p_{i,1}A)(I + p_{i,2}A)(x - x_d)}{D_i - \delta_{i,1} - \delta_{i,2}} + \mu \\ &\quad \vdots \\ h_{i,n_i,\mu}(x) &= \frac{P_i(I + p_{i,1}A) \cdots (I + p_{i,n_i}A)(x - x_d)}{D_i - \delta_{i,1} - \cdots - \delta_{i,n_i}} + \mu, \end{aligned}$$

and notice that $h_{i,j,1}$ is a positive scalar multiple of $\tilde{h}_{i,j}$. We refer to the number n_i as the depth of the above sequence. Then $I(\mu) = \{x : h_{i,j,\mu}(x) \geq 0, \forall i, \forall j\}$ forms a parameterized family of candidate invariant sets, and $I(1)$ in particular is the candidate set that enforces the conditions $P_i(x - x_d) + D_i \geq 0$. The purpose of the parameter μ is to allow one to potentially establish a region of attraction for $I(1)$ by showing that when the initial system state is in $I(\mu_{max})$ for some $\mu_{max} > 1$, the state will enter $I(\mu)$ for smaller and smaller μ over time until it reaches $I(1)$.

In order to confirm whether $I(\mu)$ is actually invariant for $\mu \in [1, \mu_{max}]$, it is sufficient to check that for all $x \in I(\mu_{max})$, we have that, for all i and j , $h_{i,j,\mu}(x) = 0$ implies that $\frac{d}{dt}(h_{i,j,\mu}(x)) > 0$. We shall refer to this implication as the invariance

condition for $h_{i,j,\mu}$. Under this condition, it is clear that the least μ satisfying $h_{i,j,\mu}(x) \geq 0$ decreases with respect to time while $\mu \geq 1$.

One may notice that under the linearized dynamics, it is only necessary to check the invariance condition for $h_{i,n_i,\mu}$ for all i , since in this case, the fact that $h_{i,n_i,\mu}(x) \geq 0$ holds implies that $h_{i,j,\mu}(x) \geq 0$ holds for all $j \leq n_i$. This continues to be true if we let $\delta_{i,j} = 0$ for all i and j . However, since we are interested in verifying invariance for the original nonlinear dynamics, it is necessary to check the invariance conditions for all functions. Also, under the nonlinear dynamics, the fact that $h_{i,j,\mu}(x) \geq 0$ holds may not automatically imply that $h_{i,j-1,\mu}(x) \geq 0$ for $\delta_{i,j} = 0$, though this issue can be mitigated by increasing $\delta_{i,j}$.

To conclude this section, we remark that in the case where $I(\mu)$ is proven to be invariant for $\mu \in [1, \mu_{max}]$, it is straightforward to check for an expanded region of attraction for $I(1)$ by verifying the invariance conditions for $\mu \in [\mu_{max}, \tilde{\mu}_{max}]$, where $\tilde{\mu}_{max} > \mu_{max}$; and similarly one can check to see if there are smaller invariant sets inside $I(1)$ by verifying the invariance conditions for $\mu \in [\mu_{min}, 1]$, for $\mu_{min} \in (0, 1)$. One can then in a systematic way, e.g., through a bisection method, approximate the exact μ -interval over which the invariant conditions are satisfied as accurately as desired; though SMT solving time may limit the accuracy one can feasibly obtain.

5. OCTOROTOR BARRIER FUNCTIONS

In this section, we describe in more detail the form of the barrier functions we use for the octorotor system. As mentioned above, the approximating linear dynamics we use is the linearization around $s = 0$. Conveniently, this approximation decomposes into 4 subsystems. The first subsystem consists of only the vertical velocity v_z . The nonlinear equation governing v_z , without disturbances, is

$$\dot{v}_z = g - \frac{F}{m} c_\phi c_\theta,$$

which, when combined with the controller defined by (1), yields

$$\dot{v}_z = -\frac{K_{dz} c_\phi c_\theta}{m} (v_z - v_{z,d}).$$

(Throughout this section, we assume that $u = u_d$.) Hence, the linearized system for v_z is

$$\dot{v}_z = -\frac{K_{dz}}{m} (v_z - v_{z,d}).$$

One of our goals is to ensure that $|v_z - v_{z,d}| \leq D_{v_z}$ for some constant $D_{v_z} > 0$, assuming the bound $|v_{z,d}| \leq D_{v_{z,d}}$ with $D_{v_{z,d}} > 0$. So we define our barrier function components for v_z by

$$h_{v_z,\mu}^\pm(s, v_z, d) = \pm \frac{v_z - v_{z,d}}{D_{v_z}} + \mu,$$

one barrier function corresponding to $+$ and one to $-$. This means that we do not make use of barrier functions of higher depth to enforce $|v_z - v_{z,d}| \leq D_{v_z}$.

The next subsystem consists of the roll angle and rate (ϕ, Ω_1) . The nonlinear equations governing these variables, without disturbances, are

$$\dot{\phi} = \Omega_1 + t_\theta (s_\phi \Omega_2 + c_\phi \Omega_3), \quad \dot{\Omega}_1 = \frac{\tau_1 + \Omega_2 \Omega_3 (J_2 - J_3)}{J_1}.$$

Linearizing and combining with the controller (1) yields

$$\dot{\phi} = \Omega_1, \quad \dot{\Omega}_1 = \frac{-K_{p\phi}(\phi - \phi_d) - K_{d\phi}\Omega_1}{J_1}.$$

Another goal is to ensure that $|\phi - \phi_d| \leq D_\phi$ for some $D_\phi > 0$, assuming that $|\phi_d| \leq D_{\phi_d}$, $D_{\phi_d} > 0$, and we aim to enforce the first inequality with barrier function sequences of depth 1. So for constants $p_{\phi,1}, \delta_{\phi,1} \geq 0$ with $\delta_{\phi,1} < D_\phi$, we define our barrier function components for (ϕ, Ω_1) as the following:

$$h_{\phi,0,\mu}^\pm(s, \phi_d) = \pm \frac{\phi - \phi_d}{D_\phi} + \mu,$$

$$h_{\phi,1,\mu}^\pm(s, \phi_d) = \pm \frac{\phi - \phi_d + p_{\phi,1}\Omega_1}{D_\phi - \delta_{\phi,1}} + \mu.$$

There are two remaining subsystems, one of which consists of the pitch angle and rate (θ, Ω_2) , and the other consists of the yaw angle and rate (ψ, Ω_3) . Both subsystems are very similar to that of the roll angle and rate. The nonlinear equations governing the dynamics of these variables are

$$\dot{\theta} = c_\phi\Omega_2 - s_\phi\Omega_3, \quad \dot{\psi} = \frac{s_\phi\Omega_2 + c_\phi\Omega_3}{c_\theta}$$

$$\dot{\Omega}_2 = \frac{\tau_2 + \Omega_1\Omega_3(J_3 - J_1)}{J_2}, \quad \dot{\Omega}_3 = \frac{\tau_3 + \Omega_1\Omega_2(J_1 - J_2)}{J_3}.$$

Linearizing and then combining these equations with the controller (1) yields

$$\dot{\theta} = \Omega_2, \quad \dot{\Omega}_2 = \frac{-K_{p\theta}(\theta - \theta_d) - K_{d\theta}\Omega_2}{J_2}$$

$$\dot{\psi} = \Omega_3, \quad \dot{\Omega}_3 = \frac{-K_{p\psi}(\psi - \psi_d) - K_{d\psi}\Omega_3}{J_3}.$$

Our goals for these variables is to ensure that $|\theta - \theta_d| \leq D_\theta$ and $|\psi - \psi_d| \leq D_\psi$ for some $D_\theta, D_\psi > 0$, assuming that $|\theta_d| \leq D_{\theta_d}$ and $|\psi_d| \leq D_{\psi_d}$, $D_{\theta_d}, D_{\psi_d} > 0$. As with the roll angle and rate, we utilize barrier function sequences of depth 1. So for constants $p_{\theta,1}, \delta_{\theta,1}, p_{\psi,1}, \delta_{\psi,1} \geq 0$ with $\delta_{\theta,1} < D_\theta$ and $\delta_{\psi,1} < D_\psi$, we define the barrier function components for (θ, Ω_2) and (ψ, Ω_3) as the following:

$$h_{\theta,0,\mu}^\pm(s, \theta_d) = \pm \frac{\theta - \theta_d}{D_\theta} + \mu,$$

$$h_{\theta,1,\mu}^\pm(s, \theta_d) = \pm \frac{\theta - \theta_d + p_{\theta,1}\Omega_2}{D_\theta - \delta_{\theta,1}} + \mu$$

$$h_{\psi,0,\mu}^\pm(s, \psi_d) = \pm \frac{\psi - \psi_d}{D_\psi} + \mu,$$

$$h_{\psi,1,\mu}^\pm(s, \psi_d) = \pm \frac{\psi - \psi_d + p_{\psi,1}\Omega_3}{D_\psi - \delta_{\psi,1}} + \mu.$$

Lastly, we also include the following functions to ensure bounds of the form $|\Omega_1| \leq D_{\Omega_1}$, $|\Omega_2| \leq D_{\Omega_2}$, and $|\Omega_3| \leq D_{\Omega_3}$, where $D_{\Omega_1}, D_{\Omega_2}, D_{\Omega_3} > 0$:

$$\begin{aligned} h_{\Omega_1, \mu}^{\pm}(s) &= \pm \frac{\Omega_1}{D_{\Omega_1}} + \mu, \\ h_{\Omega_2, \mu}^{\pm}(s) &= \pm \frac{\Omega_2}{D_{\Omega_2}} + \mu, \\ h_{\Omega_3, \mu}^{\pm}(s) &= \pm \frac{\Omega_3}{D_{\Omega_3}} + \mu. \end{aligned}$$

This completes the description of all the barrier functions.

6. VERIFICATION PROCESS

We will now formulate the statements about the octorotor system that we formally analyze in dReal. The dReal SMT solver [6] is capable of analyzing statements in the theory of first-order real arithmetic with non-linear function symbols (including, crucially, transcendental functions) in order to determine their satisfiability. In order to overcome well-known decidability issues with this theory, dReal incorporates a numerical precision constant that mediates the granularity of the proof search. Given a statement φ in this theory, dReal will reply with one of the following:

- An assignment of ranges (intervals) to the (free) variables of φ that make the statement satisfiable modulo the numerical precision; or
- A proof that there is no assignment that would make φ satisfiable.

The first case is referred to as a δ -SAT result. The second case is referred to as an UNSAT result. In general, it is not possible to determine, given the assignment corresponding to a δ -SAT result whether or not there are values in the range of the assignment that would make the statement satisfiable. However, one can sample from these intervals and evaluate the results in order to further search for a genuinely satisfiable (SAT) result. In practice, when running dReal we always carry out a naïve search within δ -SAT ranges by polling the midpoint of the returned box. Thus, in the sequel SAT means that we have found a genuine counter-example via this further polling of the variable ranges returned as part of one of dReal's δ -SATs. We always formulate safety properties in such a way that the goal is to obtain an UNSAT result, i.e., a proof of unsatisfiability, from dReal.

First, we introduce a constant ϵ , a small positive number that we use for various purposes, one of which is to make our safety conditions slightly more strict to account for potential numerical errors. Next, we define a search space over which the statements we formulate are proven. In particular, we restrict all of the following variables to a symmetric interval about 0:¹

$$v_z, \phi, \theta, \psi, \Omega_1, \Omega_2, \Omega_3, \Delta_z, \Delta_{R,1}, \Delta_{R,2}, \Delta_{R,3}, v_{z,d}, \phi_d, \theta_d, \psi_d.$$

That is, for all variables ξ above, we restrict ξ to lie in the interval $(-\xi_{max}, \xi_{max})$, where $\xi_{max} > 0$. We also restrict the variable μ to the interval $(1 - \epsilon, \mu_{max} + \epsilon)$. This ensures that dReal conducts a well bounded search, which avoids unnecessary computational issues. As mentioned above, all conditions are expressed in terms of

¹The regions could be asymmetric and for other kinds of tasks that might be more natural. For the task at hand, symmetry of the regions is most reasonable.

a search for a state which *violates* the desired safety condition. The aim is then to use dReal to verify that such a violation cannot exist, which proves the condition.

6.1. Barrier function support is inside search space. Now the first thing we wish to ensure is that the common support of the barrier functions we define is a subset of our search space. This is because it is necessary to search over the full boundary of the support when checking invariance. For this property, we formulate the dReal search as follows. We search for a state s near the boundary of the search space —i.e., satisfying $\xi > \xi_{max} - \epsilon$ or $\xi < -\xi_{max} + \epsilon$ for some $\xi \in \{v_z, \phi, \theta, \psi, \Omega_1, \Omega_2, \Omega_3\}$ — such that there exists a barrier function component h and, if needed, associated command c such that s is in or near the support of $h(\cdot, c)$, i.e., $h(s, c) > -\epsilon$. If h has no argument for a command c , then the last inequality should be replaced by $h(s) > -\epsilon$. If dReal verifies that no such state s exists, then we can conclude that the full support is inside the search space.

6.2. Invariance of barrier function support. Next, we formulate the conditions for checking that the barrier function support is invariant, and we do this by checking the invariance property for each barrier function component. Here we are assuming that the controller defined by (1) always works, i.e., $u = u_d$ and we disregard the rotor thrust limits. Also, we assume that the states s we search over are in or near the support of every barrier function component, i.e., for all barrier function components h , we have $h(s, c) > -\epsilon$ for some associated command c , if such a command is needed, or otherwise $h(s) > -\epsilon$. With these assumptions in mind, we formulate one condition for each barrier function component. For the component h_* , we search for a state s and, if needed, a command c associated with h_* such that s is on or near the boundary of the support of $h_*(\cdot, c)$ (or $h_*(s)$), i.e., $-\epsilon < h_*(s, c) < \epsilon$ (or $-\epsilon < h_*(s) < \epsilon$), and the time derivative of $h_*(s, c)$ (or $h_*(s)$) is almost negative, i.e., $\frac{d}{dt}(h_*(s, c)) < \epsilon$ (or $\frac{d}{dt}(h_*(s)) < \epsilon$). For the sake of clarity, the condition we impose on the state s to consider it a violation of the invariance condition for h_* is the following:

$$\left(\begin{array}{l} \text{for every b.f. component } h, \text{ there exists an} \\ \text{associated command } c \text{ such that } h(s, c) > -\epsilon \end{array} \right) \\ \wedge \left(\begin{array}{l} \text{there exists a command } c \text{ associated to } h_* \\ \text{such that } h_*(s, c) < \epsilon \text{ and } \frac{d}{dt}(h_*(s, c)) < \epsilon \end{array} \right).$$

For h or h_* that has no argument for a command in the above expression, we disregard the corresponding command c and replace $h(s, c)$ with $h(s)$, or $h_*(s, c)$ with $h_*(s)$. If, for every barrier function component h_* , there is no state s that satisfies the above condition, then the barrier function support is invariant under the controller defined by (1).

6.3. Rotor thrust bounds. The last condition we check is the equality $u = u_d$ we assumed in the previous condition. More specifically, we wish to check whether this equality is true over the support of the given barrier function and under the rotor failure combination being considered. As explained in Section 3.2, it suffices to check whether the thrusts \tilde{f}_j of the non-failed rotors given by the allocation method are valid and stay within the interval $[f_{min}, f_{max}]$, that is, as long as $\text{rank}(\Lambda_W) = 4$. We formulate a condition for each combination of rotor failures, so let $W \subseteq \{1, \dots, 8\}$ such that $\text{rank}(\Lambda_W) = 4$. It is clear we can consider u_d a function of s by definition; and as a result, by (2) we can view \tilde{f}_{all} as a function

of s . With this in mind, we can formulate our search as follows. We search for a state s such that for every barrier function component h , $h(s, c) > -\epsilon$ for some corresponding command c (or $h(s) > -\epsilon$), and additionally, for some $j \notin W$, \tilde{f}_j is outside, or nearly outside, of $[f_{min}, f_{max}]$, i.e., $\tilde{f}_j - f_{max} > -\epsilon$ or $\tilde{f}_j - f_{min} < \epsilon$. If dReal verifies that no such state s exists, then the octorotor controller behaves as intended for the rotor failure combination being analyzed.

7. RESULTS

We apply our verification process to an octorotor model with the characteristics of that in [14]. Specifically, the octorotor model has mass $m = 1.2$ kg, inertia matrix entries $J_1 = J_2 = 7.5 \times 10^{-3}$ kg · m² and $J_3 = 1.3 \times 10^{-2}$ kg · m², arm length $d = 0.4$ m, and torque-to-thrust ratio $c = (\frac{7.5}{3.13}) \times 10^{-2}$ m. Additionally, we let the minimum and maximum rotor thrusts be $f_{min} = 0$ and $f_{max} = \frac{1}{2}mg$, and let the maximum disturbance magnitudes be $\Delta_{r,max} = \frac{1}{10}mg$, $\Delta_{R,12,max} = (0.6 \frac{\text{rad}}{\text{s}^2})J_1$, and $\Delta_{R,3,max} = (0.6 \frac{\text{rad}}{\text{s}^2})J_3$.

Next, to find the coefficients of the controller (1), we compute the linear quadratic regulator for the linearization of the octorotor system at $s = 0$, while assuming that $s_d = 0$ and neglecting the disturbances Δ_r, Δ_R . Specifically, we find the linear controller that minimizes the objective function

$$\int_0^\infty (s^T Q s + |u|^2) dt,$$

with $Q = \text{diag} \left(40, \frac{1}{4}, \frac{1}{4}, \frac{1}{4}, \frac{1}{8}, \frac{1}{8}, \frac{1}{8} \right)$,

under the linearized dynamics. The resulting coefficients in (1) are then (approximately) as follows:

$$(3) \quad \begin{aligned} K_{dz} &= 6.32, & K_{p\phi} &= K_{p\theta} = K_{p\psi} = 0.5, \\ K_{d\phi} &= K_{d\theta} = 0.364, & K_{d\psi} &= 0.371. \end{aligned}$$

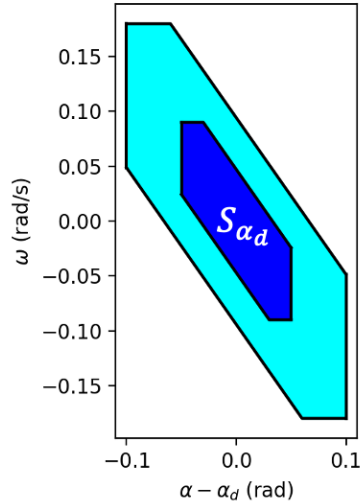
Next, to define the barrier function components, we make the following assignments:

$$\begin{aligned} D_{v_z} &= 0.25, & D_{v_{z,d}} &= 1, & D_\phi &= D_\theta = D_\psi = 0.05, \\ D_{\phi_d} &= D_{\theta_d} = 0.15, & D_{\psi_d} &= \epsilon, & D_{\Omega_1} &= D_{\Omega_2} = D_{\Omega_3} = 0.09, \\ p_{\phi,1} &= p_{\theta,1} = p_{\psi,1} = 0.7, & \delta_{\phi,1} &= \delta_{\theta,1} = \delta_{\psi,1} = 0.017, \\ \mu_{max} &= 2. \end{aligned}$$

This means that the command $v_{z,d}$ is allowed to span the interval $(-1, 1)$, and ϕ_d and θ_d are allowed to span $(-0.15, 0.15)$. Note that there is no loss in letting $D_{\psi_d} = \epsilon$, hence $\psi_d \approx 0$, since one can always redefine coordinates so that $\psi_d = 0$. Also, for any combination of commands, the candidate invariant set resulting from the barrier functions is the set $I(1)$ of states s such that $|v_z - v_{z,d}| \leq 0.25$, $(\phi, \Omega_1) \in S_{\phi_d}$, $(\theta, \Omega_2) \in S_{\theta_d}$, and $(\psi, \Omega_3) \in S_{\psi_d}$, where

$$S_{\alpha_d} = \left\{ (\alpha, \omega) \in \mathbb{R}^2 : \begin{aligned} &|\alpha - \alpha_d| \leq 0.05, |\omega| \leq 0.09 \\ &|\alpha - \alpha_d + 0.7\omega| \leq 0.033 \end{aligned} \right\}.$$

The set S_{α_d} is the dark blue region illustrated in Figure 3. The light blue region is the dilation of S_{α_d} by a factor of 2, and corresponds to the region of attraction for the invariant set. Lastly, we let $\epsilon = 10^{-8}$.

FIGURE 3. The region S_{α_d}

With all of the above definitions, we used dReal to obtain a proof of safety in the case of no rotor failures, as well as many combinations of rotor failures. That is, we used dReal to successfully verify that the set $I(\mu)$ is invariant for $1 \leq \mu \leq 2$ under the controller (1) with coefficients (3), and that the octorotor is capable of executing the controller's actions under various rotor failure combinations. Table 1 shows the times it took to prove the various conditions that ensure safety in the case where there are no rotor failures. Recall that UNSAT cases correspond to safety proofs found and SAT cases correspond to concrete counter-examples found. (Note that there is a small discrepancy between the sum of the times of the individual steps and the total time since the latter is the run time for a single script that performed all the steps in the table, and a small portion of the script is not taken into account in the recorded times for the steps.) Additionally, Table 2 shows the various times it takes to check whether the individual rotor thrusts \tilde{f}_j stay in $[f_{min}, f_{max}]$ for various rotor failure combinations, in which failed rotors exert zero thrust, i.e., they experience complete failures. In particular, note that the octorotor remains safe for up to two rotor failures, except when the failures occur on adjacent rotors that rotate the same direction. Lastly, Table 3 shows the times it takes to check the individual rotor thrust bounds for rotor failures where the thrusts of failed rotors can get stuck at zero or nonzero values. (Note that $\mu_{max} = 2$ for all entries except where μ_{max} is specified, in which case μ_{max} was decreased in order to obtain an UNSAT.) All times were obtained using 16 cores.

8. CONCLUSION

This paper introduces a framework for the formal verification of the safety of control systems using exponential barrier functions, with the target application of ensuring the faithful command tracking of an octorotor controller. Our method uses barrier functions to construct candidate invariant sets for the octorotor dynamics,

TABLE 1. Run times for checking safety conditions for no rotor failures

Step	Precision	SAT/UNSAT	Proof times (with 16 cores)		
			real	user	sys
Search space contains b.f. support	10^{-2}	UNSAT	0m0.015s	-	-
Invariance, v_z b.f. components	10^{-2}	UNSAT	0m0.165s	-	-
Invariance, ϕ, Ω_1 b.f. components	10^{-2}	UNSAT	253m20.942s	-	-
Invariance, θ, Ω_2 b.f. components	10^{-2}	UNSAT	253m41.323s	-	-
Invariance, ψ, Ω_3 b.f. components	10^{-2}	UNSAT	0m0.055s	-	-
Rotor bounds (no rotor failures)	10^{-2}	UNSAT	0m0.109s	-	-
Total time			507m3.938s	7576m43.915s	443m29.505s

TABLE 2. Run times for checking rotor bounds with complete rotor failures

Step: Rotor bounds under failures	Precision	SAT/UNSAT	Proof times (with 16 cores)		
			real	user	sys
Rotor 1 complete failure	10^{-2}	UNSAT	0m0.925s	0m5.847s	0m4.571s
Rotor 1, 2 complete failures	10^{-5}	SAT	0m0.818s	0m4.810s	0m4.687s
Rotor 1, 3 complete failures	10^{-2}	UNSAT	0m0.923s	0m5.823s	0m4.594s
Rotor 1, 4 complete failures	10^{-2}	UNSAT	0m0.910s	0m5.870s	0m4.416s
Rotor 1, 5 complete failures	10^{-2}	UNSAT	0m0.803s	0m4.179s	0m3.971s
Rotor 1, 6 complete failures	10^{-2}	UNSAT	0m0.898s	0m5.660s	0m4.343s
Rotor 1, 7 complete failures	10^{-2}	UNSAT	0m0.893s	0m5.723s	0m4.313s
Rotor 1, 8 complete failures	10^{-2}	UNSAT	0m1.035s	0m6.969s	0m4.322s

and invariance of these sets are then formally checked by the SMT solver dReal. We account for potential rotor failures through a pseudo-inverse control allocator, which we also verify to produce valid rotor thrusts via dReal. Using our approach, we verify that a particular controller causes the oct rotor to follow commands within a certain margin of error under dynamic disturbances and several types of rotor failures. Our approach is fairly general, and can potentially be used to construct safe invariant sets in many different systems and using different kinds of controllers. One particularly promising application is in the verification of gain scheduled controllers for aircraft.

REFERENCES

- [1] H. Alwi and C. Edwards. Fault tolerant control of an oct rotor using LPV based sliding mode control allocation. In *2013 American Control Conference*, pages 6505–6510, 2013.
- [2] H. Alwi and C. Edwards. Sliding mode fault-tolerant control of an oct rotor using linear parameter varying-based schemes. *IET Control Theory and Applications*, 9(4):618–636, 2015.
- [3] A. D. Ames, S. Coogan, M. Egerstedt, G. Notomista, K. Sreenath, and P. Tabuada. Control barrier functions: Theory and applications. In *2019 18th European Control Conference (ECC)*, pages 3420–3431, 2019.
- [4] A. D. Ames, X. Xu, J. W. Grizzle, and P. Tabuada. Control barrier function based quadratic programs for safety critical systems. *IEEE Transactions on Automatic Control*, 62(8):3861–3876, 2017.
- [5] A. Freddi, A. Lanzon, and S. Longhi. A feedback linearization approach to fault tolerance in quadrotor vehicles. In *Proceedings of the 18th IFAC World Congress*, pages 5413–5418, 2011.
- [6] Sicun Gao, Soonho Kong, and Edmund M Clarke. dreal: An smt solver for nonlinear theories over the reals. In *International conference on automated deduction*, pages 208–214. Springer, 2013.

TABLE 3. Run times for checking rotor bounds with stuck rotor failures

Step: Rotor bounds under failures	Precision	SAT/UNSAT	Proof times (with 16 cores)		
			real	user	sys
Rotor 1 thrust stuck at $\frac{mg}{8}$	10^{-2}	UNSAT	0m0.946s	0m5.245s	0m4.499s
Rotor 1 thrust stuck at $\frac{mg}{6}, \mu_{max} = 1.6$	10^{-2}	UNSAT	0m2.267s	0m25.905s	0m4.608s
Rotor 1, 2 thrusts stuck at $0, \frac{mg}{8}$	10^{-2}	SAT	0m0.932s	0m3.660s	0m3.644s
Rotor 1, 2 thrusts stuck at $\frac{mg}{8}, \frac{mg}{8}, \mu_{max} = 1.5$	10^{-2}	UNSAT	0m7.261s	1m45.881s	0m5.297s
Rotor 1, 2 thrusts stuck at $0, \frac{mg}{6}$	10^{-5}	SAT	0m0.887s	0m5.530s	0m4.155s
Rotor 1, 2 thrusts stuck at $\frac{mg}{6}, \frac{mg}{6}$	10^{-4}	SAT	0m0.883s	0m3.833s	0m3.820s
Rotor 1, 3 thrusts stuck at $0, \frac{mg}{8}, \mu_{max} = 1.6$	10^{-2}	UNSAT	0m10.498s	2m37.854s	0m4.288s
Rotor 1, 3 thrusts stuck at $\frac{mg}{8}, \frac{mg}{8}$	10^{-2}	UNSAT	0m1.270s	0m9.844s	0m3.996s
Rotor 1, 3 thrusts stuck at $0, \frac{mg}{6}$	10^{-6}	SAT	0m0.863s	0m3.947s	0m4.064s
Rotor 1, 3 thrusts stuck at $\frac{mg}{6}, \frac{mg}{6}, \mu_{max} = 1.3$	10^{-2}	UNSAT	0m22.850s	5m51.932s	0m6.821s
Rotor 1, 8 thrusts stuck at $0, \frac{mg}{8}$	10^{-2}	UNSAT	0m1.037s	0m6.810s	0m4.310s
Rotor 1, 8 thrusts stuck at $\frac{mg}{8}, \frac{mg}{8}$	10^{-2}	UNSAT	0m3.899s	0m51.320s	0m4.599s
Rotor 1, 8 thrusts stuck at $0, \frac{mg}{6}$	10^{-2}	UNSAT	0m1.502s	0m13.834s	0m4.068s
Rotor 1, 8 thrusts stuck at $\frac{mg}{6}, \frac{mg}{6}, \mu_{max} = 1.1$	10^{-2}	UNSAT	0m8.274s	2m0.787s	0m5.040s

- [7] F. Goodarzi, D. Lee, and T. Lee. Geometric nonlinear PID control of a quadrotor UAV on SE(3). In *2013 European Control Conference (ECC)*, pages 3845–3850, 2013.
- [8] G. Hoffmann, H. Huang, S. Waslander, and C. Tomlin. Quadrotor helicopter flight dynamics and control: Theory and experiment. In *Proceedings of the AIAA Guidance, Navigation, and Control Conference*, 2007.
- [9] O. A. Jasim and S. M. Veres. Formal verification of quadcopter flight envelop using theorem prover. In *2018 IEEE Conference on Control Technology and Applications (CCTA)*, pages 1502–1507, 2018.
- [10] O. A. Jasim and S. M. Veres. Nonlinear attitude control design and verification for a safe flight of a small-scale unmanned helicopter. In *2019 6th International Conference on Control, Decision and Information Technologies (CoDIT)*, pages 1652–1657, 2019.
- [11] M. Khan, M. Zafar, and A. Chatterjee. Barrier functions in cascaded controller: Safe quadrotor control. In *2020 American Control Conference (ACC)*, pages 1737–1742, 2020.
- [12] T. Lee, M. Leok, and N. H. McClamroch. Nonlinear robust tracking control of a quadrotor UAV on SE(3). *Asian Journal of Control*, 15(2):391–408, 2013.
- [13] R. Mahony, V. Kumar, and P. Corke. Multirotor aerial vehicles: Modeling, estimation, and control of quadrotor. *IEEE Robotics Automation Magazine*, 19(3):20–32, 2012.
- [14] A. Marks, J. F. Whidborne, and I. Yamamoto. Control allocation for fault tolerant control of a VTOL octorotor. In *Proceedings of 2012 UKACC International Conference on Control*, pages 357–362, 2012.
- [15] Q. Nguyen, A. Hereid, J. W. Grizzle, A. D. Ames, and K. Sreenath. 3D dynamic walking on stepping stones with control barrier functions. In *2016 IEEE 55th Conference on Decision and Control (CDC)*, pages 827–834, 2016.
- [16] Q. Nguyen and K. Sreenath. Safety-critical control for dynamical bipedal walking with precise footstep placement. In *IFAC Analysis and Design of Hybrid Systems*, pages 147–154, 2015.
- [17] Q. Nguyen and K. Sreenath. Exponential control barrier functions for enforcing high relative-degree safety-critical constraints. In *2016 American Control Conference (ACC)*, pages 322–328, 2016.
- [18] P. Nilsson and A. D. Ames. Barrier functions: Bridging the gap between planning from specifications and safety-critical control. In *2018 IEEE Conference on Decision and Control (CDC)*, pages 765–772, 2018.
- [19] M. W. Oppenheimer, D. B. Doman, and M. A. Bolender. Control allocation for over-actuated systems. In *2006 14th Mediterranean Conference on Control and Automation*, 2006.
- [20] M. Ranjbaran and K. Khorasani. Fault recovery of an under-actuated quadrotor aerial vehicle. In *49th IEEE Conference on Decision and Control (CDC)*, pages 4385–4392, 2010.

- [21] M. Saied, B. Lussier, I. Fantoni, C. Francis, H. Shraim, and G. Sanahuja. Fault diagnosis and fault-tolerant control strategy for rotor failure in an octorotor. In *2015 IEEE International Conference on Robotics and Automation (ICRA)*, pages 5266–5271, 2015.
- [22] M. Saied, B. Lussier, I. Fantoni, H. Shraim, and C. Francis. Fault diagnosis and fault-tolerant control of an octorotor UAV using motors speeds measurements. *20th IFAC World Congress*, pages 5263–5268, 2017.
- [23] F. Sharifi, M. Mirzaei, B. W. Gordon, and Y. Zhang. Fault tolerant control of a quadrotor uav using sliding mode control. In *2010 Conference on Control and Fault-Tolerant Systems (SysTol)*, pages 239–244, 2010.
- [24] L. Wang, A. D. Ames, and M. Egerstedt. Safe certificate-based maneuvers for teams of quadrotors using differential flatness. In *2017 IEEE International Conference on Robotics and Automation (ICRA)*, pages 3293–3298, 2017.
- [25] L. Wang, A. D. Ames, and M. Egerstedt. Safety barrier certificates for collisions-free multi-robot systems. *IEEE Transactions on Robotics*, 33(3):661–674, 2017.
- [26] L. Wang, E. A. Theodorou, and M. Egerstedt. Safe learning of quadrotor dynamics using barrier certificates. In *2018 IEEE International Conference on Robotics and Automation (ICRA)*, pages 2460–2465, 2018.
- [27] G. Wu and K. Sreenath. Safety-critical control of a 3D quadrotor with range-limited sensing. In *ASME 2016 Dynamic Systems and Control Conference*, 2016.
- [28] B. Xu and K. Sreenath. Safe teleoperation of dynamic UAVs through control barrier functions. In *2018 IEEE International Conference on Robotics and Automation (ICRA)*, pages 7848–7855, 2018.
- [29] X. Xu, J. W. Grizzle, P. Tabuada, and A. D. Ames. Correctness guarantees for the composition of lane keeping and adaptive cruise control. *IEEE Transactions on Automation Science and Engineering*, 15(3):1216–1229, 2018.
- [30] X. Xu, T. Waters, D. Pickem, P. Glotfelter, M. Egerstedt, P. Tabuada, J. W. Grizzle, and A. D. Ames. Realizing simultaneous lane keeping and adaptive speed regulation on accessible mobile robot testbeds. In *2017 IEEE Conference on Control Technology and Applications (CCTA)*, pages 1769–1775, 2017.
- [31] Y. Zhang and A. Chamseddine. Fault tolerant flight control techniques with application to a quadrotor UAV testbed. In T. Lombaerts, editor, *Automatic Flight Control Systems - Latest Developments*, pages 119–150. InTech, 2012.
- [32] Q. Zhou, Y. Zhang, C. Rabbath, and D. Theilliol. Design of feedback linearization control and reconfigurable control allocation with application to a quadrotor UAV. In *2010 Conference on Control and Fault-Tolerant Systems (SysTol)*, pages 371–376, 2010.